Supporting Information

Bright $CsPbI_3$ Perovskite Quantum Dot Light-Emitting Diodes with Top-Emitting Structure and a Low Efficiency Roll-Off Realized by Applying Zirconium Acetylacetonate Surface Modification

Min Lu,[†,#] Jie Guo,[†,#] Siqi Sun,[†] Po Lu,[†] Jinlei Wu,[†] Yu Wang,[†] Stephen V. Kershaw,[§] William W. Yu,*[,†,‡] Andrey L. Rogach,*[,§] and Yu Zhang*[,†]

[†]State Key Laboratory of Integrated Optoelectronics, College of Electronic Science and Engineering, Jilin University, Changchun 130012, China

[‡]Department of Chemistry and Physics, Louisiana State University, Shreveport, LA 71115, USA

[§]Department of Materials Science and Engineering, and Centre for Functional Photonics (CFP), City University of Hong Kong, Kowloon, Hong Kong SAR

Experimental Section

Materials: Oleic acid (OA, 90%) and 1-octadecene (ODE, 90%) were purchased from Alfa Aesar. Oleylamine (OLA, 80-90%), PbO_2 (99.999%), NH_4I (99.999%), zirconium acetylacetonate (98%) and polyethyleneimine (PEI, 99%) were purchased from Aladdin. Cs_2CO_3 (99.9%) and 2-methoxyethanol (99%) were purchased from J&K. All materials were used as received.

Synthesis of perovskite QDs: Cesium oleate was prepared by adding Cs_2CO_3 (2.50 mmol), OA (2.5 mL), and ODE (30.0 mL) into a 100 mL three-neck flask; the mixture was degassed and dried under vacuum for 1 h at 120 ˚C, and heated to 150 ˚C under N_2 until a clear solution was obtained. For the synthesis of $CsPbI_3$ QDs with a Pb:Zr molar ratio equal to 1:0.5, 10.0 mL ODE, 0.376 mmol PbO, 1.128 mmol NH_4I, and 0.188 mmol zirconium acetylacetonate were loaded into a 50 mL three-neck flask, degassed and dried by applying vacuum for 1 h at 120 ˚C; then 2.0 mL OA and 2.0 mL OLA were injected. After the solution became clear, the temperature was raised to 165 ˚C, and 0.8 mL of cesium oleate solution was injected. Five seconds later, the reaction mixture was cooled down to room temperature in an ice-water bath. Perovskite QDs were separated by centrifugation for 10 min at 5000 rpm, re-dispersed in 2.0 mL of toluene, followed by addition of 2 mL ethyl acetate, centrifugation for 10 min at 10000 rpm, and finally redispersion in 1.0 mL of toluene.

Synthesis of ZnO nanocrystals: A mixture of zinc acetate (0.4403 g) and ethyl alcohol (30.0 mL) was loaded into a 250 mL three-neck flask, degassed at room temperature for 10 min, and heated to boiling point until the zinc acetate powder was completely dissolved. After 30 min, the flask was allowed to cool to room temperature naturally. Sodium hydroxide (0.2 g) in ethyl alcohol (10 mL) was injected into the flask, and the mixture was maintained at room temperature for 4 h. The product was purified by adding 40 mL n-hexane, followed by centrifugation for 10 min at 5000 rpm, and the finally obtained precipitate was dissolved in 3 mL of ethyl alcohol.

Device fabrication: Silicon wafers were cleaned successively using soap, deionized water, ethanol, acetone, and isopropanol. A 200 nm Ag film was deposited onto the silicon substrate via thermal evaporation, and a solution of ZnO (50 mg mL^{-1}) was spin-coated on top of the Ag film at 1000 rpm for 1 min and annealed in air at 150 ˚C for 10 min. The substrate was transferred into a N_2 glove-box, and a polyethyleneimine (PEI) 2-methoxyethanol solution (0.2%

mass fraction) was spin-coated at a speed of 3000 rpm for 1 min and annealed at 125 ˚C for 10 min. The perovskite QD emissive layer was spin-cast from a 20 mg mL^{-1} QD solution at 1000 rpm for 1 min. TCTA, MoO_3, and Au layers were sequentially deposited by thermal evaporation in a vacuum deposition clamber under a vacuum of 1×10^{-7} Torr.

Characterization: Absorption and photoluminescence (PL) spectra were measured on a Perkin Elmer Lambda 950 spectrometer and a Cary Eclipse spectrofluorimeter, respectively. Transmission electron microscopy (TEM) images were obtained on a FEI Tecnai F20 microscope. Scanning electron microscopy (SEM) images were taken on a JEOL JSM-7500F system. X-ray diffraction (XRD) data were collected on a Bruker SMART-CCD diffractometer. The absolute PL quantum yield (QY) of the samples was measured on a fluorescence spectrometer (FLS920P, Edinburgh Instruments) equipped with an integrating sphere. X-ray photoelectron spectroscopy (XPS) was done on an ESCALAB250 spectrometer. Time-resolved PL measurements were performed with a time correlated single-photon counting system on the FLS920P Edinburgh spectrometer. A 379 nm picosecond diode laser (EPL-375, repetition rate 5 MHz, pulse width 64.8 ps) was used as an excitation source. Ultraviolet photoelectron spectra (UPS) were collected using a PREVAC system. The J−V−L characteristics and the EL spectra of LEDs were collected on a Keithley 2400 source meter and a Photo Research spectrometer PR650 with an adhesive encapsulation in a dark room, respectively.

Calculation of radiative & non-radiative decay rates

The average PL lifetimes (τ_{avg}) were obtained from PL decays by using the following equation[1, 2]

$$\tau_{avg} = \frac{1}{I\ (0)} \int_0^\infty I(t)\ \ dt \qquad (1)$$

where the integration was performed numerically. The radiative and nonradiative components of the total PL decay were determined via the following equations

$$\frac{1}{K_r} = \tau_r = \frac{\tau_{avg}}{QY} \qquad (2)$$

$$\frac{1}{K_{nr}} = \tau_{nr} = \frac{\tau_{avg}}{1-QY} \qquad (3)$$

where K_r, K_{nr}, τ_r, τ_{nr} are the radiative decay rate, nonradiative decay rate, radiative lifetime, and nonradiative lifetime, respectively. Absolute PL QYs of the samples were obtained using a fluorescence spectrometer with an integrating sphere under the same excitation wavelength

(365 nm) as for the PL decay measurements.

It is noted that the Equation (3) ignores the presence of dark (not emitting) dots in the samples, which may overestimate the nonradiative decay rate.[3, 4] If the fraction of bright dots is p (< 1) and the remaining particles are completely dark on the measurement timescale (time between pulses in a TCSPC decay time experiment), Equation (3) needs to be corrected as follows:

$$\frac{1}{K_{nr}} = \tau_{nr} = \frac{\tau_{avg}}{1-QY}\ f_{cor}(p, QY),\ f_{cor}(p, QY) = \frac{1-p\times QY}{p(1-QY)} \qquad (4)$$

The correction function in Equation (4) (f_{cor} (p, QY) ≥ 1) becomes increasingly important when the fraction of dark perovskite QDs decreases.[5, 6] For low PL QY value, its dependence on the fraction of dark/bright perovskite QDs is rather weak; when the PL QY is high, the true nonradiative rate will be overestimated by some factor between 0 and 1 (but closer to 1). Dark fraction measurements have been made via QD emission blinking experiments on single isolated QDs cast from dilute solutions onto solid substrates (i.e. as dry isolated QDs), or in dilute aqueous solutions in other cases. [5, 6] However, such measurements are not routinely available either for more concentrated organic solvent solutions or indeed the solid packed QD films used in LEDs. In the absence of a definitive measurement of f_{cor} (p, QY), it is only possible to comment on relative trends in K_{nr} using Equation (3), with the tacit assumption that the overestimation due to ignoring the dark fraction is not changing significantly across a set of samples. This is probably a less valid assumption when the PL QY is closer to 100%, and the dark fraction is also influenced by the same material properties as those that govern the PL QY.

Table S1. PL characteristics, including PL QYs, PL average lifetimes (τ_{avg}), radiative decay rates (K_r), and apparent (determined by using Equation (3)) nonradiative decay rates (K_{nr}) of the $CsPbI_3$ QDs with different Pb:Zr ratios.

Molar ratio	**PL QY (%)**	**τ_{avg} (ns)**	**K_r ($\times 10^6$ s^{-1})**	**K_{nr} ($\times 10^6$ s^{-1})**
Pb:Zr=1:0	70	50.8	13.9	5.9
Pb:Zr=1:0.5	82	53.9	15.2	3.3
Pb:Zr=1:1	91	58.8	15.5	1.5
Pb:Zr=1:2	75	48.3	15.5	5.2

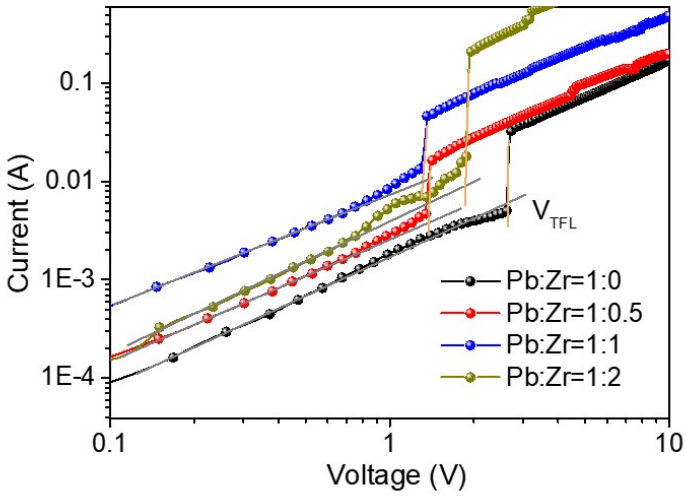

Figure S1. Trap density extraction for the $CsPbI_3$ QD samples treated with different amount of Zr, determined by dark current-voltage measurements on electron-only devices with the structure of ITO/perovskite/TPBi/LiF/Al. Gray lines represent the ohmic regime of each case, and the orange lines represent the trap-filled limit (TFL) regime and the onset voltage (V_{TFL}).

Table S2. The onset voltage (V_{TFL}) and the trap density (N_t) of the $CsPbI_3$ QD films with different Pb:Zr ratios.

Molar ratio	V_{TFL} (V)	N_t (cm^{-3})
Pb:Zr=1:0	2.63	1.28×10^{17}
Pb:Zr=1:0.5	1.38	6.70×10^{16}
Pb:Zr=1:1	1.31	6.36×10^{16}
Pb:Zr=1:2	1.87	9.08×10^{16}

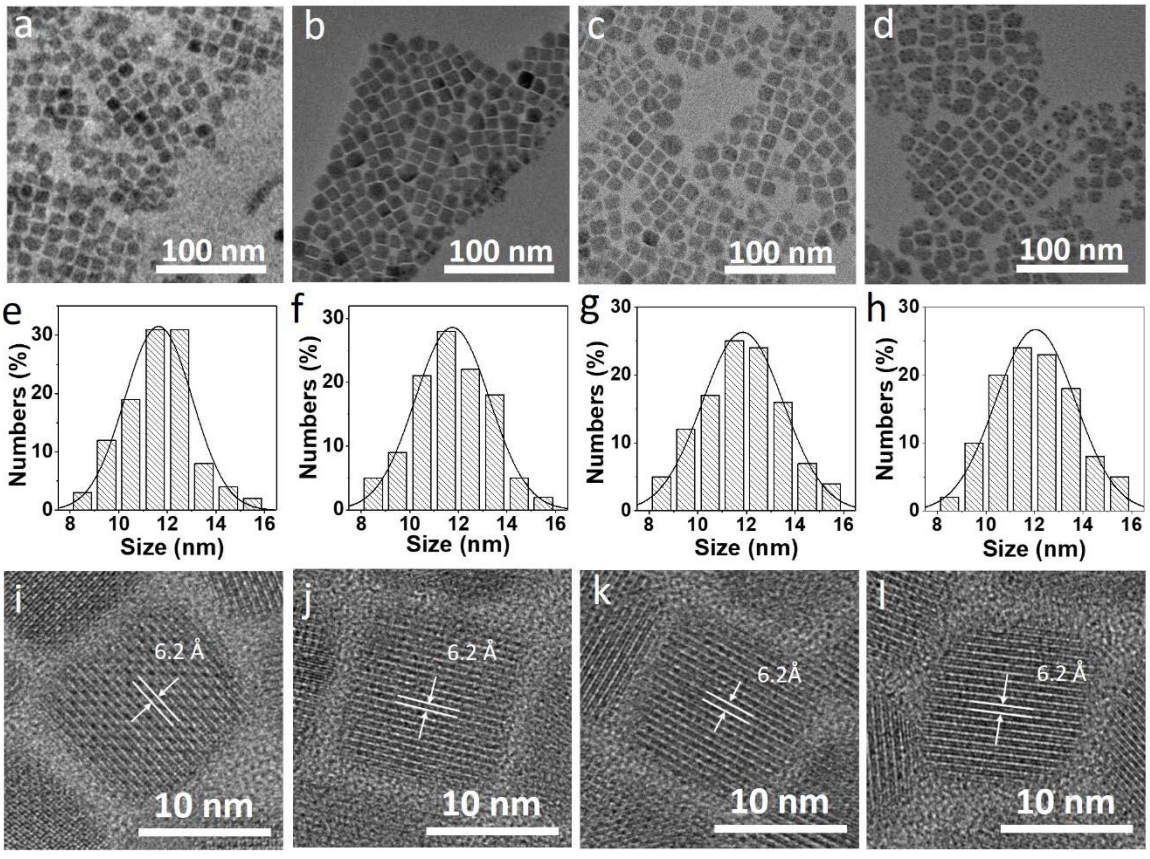

Figure S2. (a-d) TEM images, (e-h) corresponding size distribution histograms, and (i-l) corresponding HRTEM images of $CsPbI_3$ QDs synthesized using different Pb:Zr ratios (1:0, 1:0.5, 1:1, and 1:2, respectively).

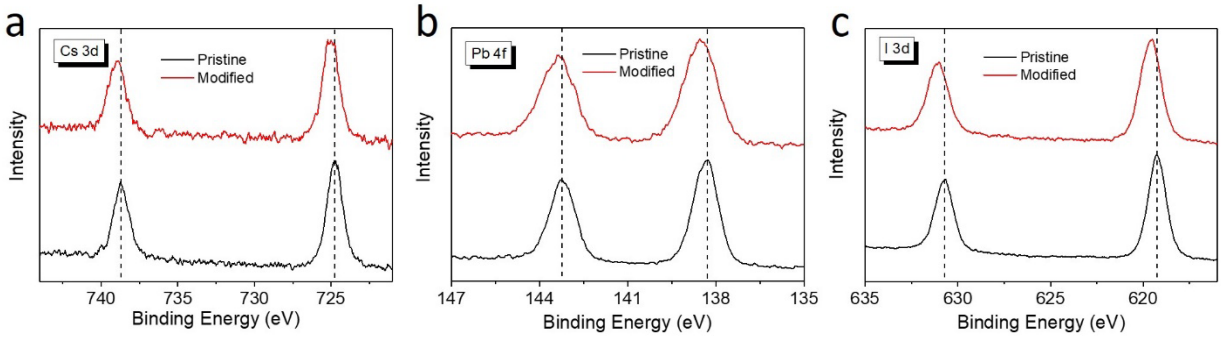

Figure S3. High-resolution XPS spectra of pristine $CsPbI_3$ QDs (i.e. Pb:Zr = 1:0) and Zr modified $CsPbI_3$ QDs with Pb:Zr = 1:1 for (a) Cs 3d, (b) Pb 4f, and (c) I 3d.

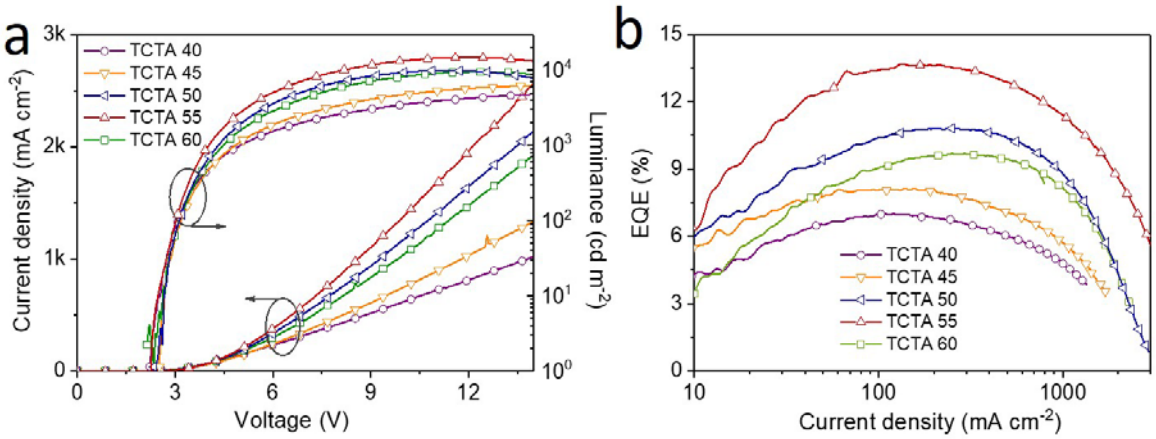

Figure S4. (a) Current density and luminance *versus* driving voltage, and (b) external quantum efficiency *versus* current density of the Zr-modified $CsPbI_3$ top-emitting Pe-QLEDs with different thicknesses of TCTA layer.

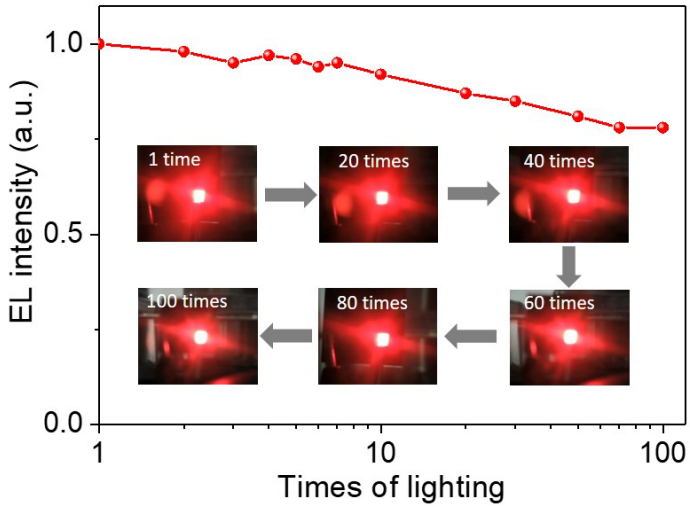

Figure S5. Change of the EL intensity during repeated operation cycling (with drive conditions as described in the main text) of the Zr-modified $CsPbI_3$ top-emitting Pe-QLEDs, in a glove box, together with representative photographs of operating devices.

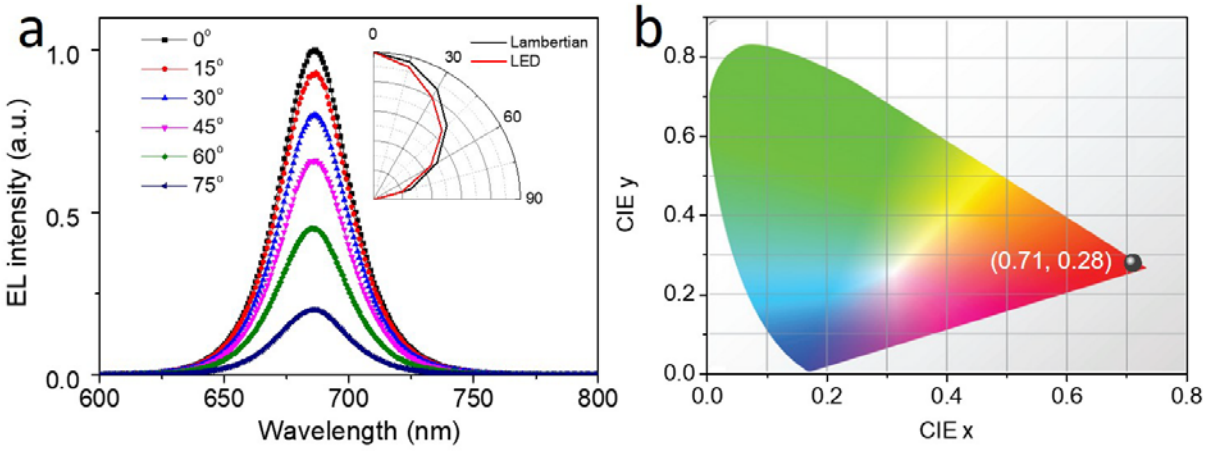

Figure S6. (a) EL spectra of Zr-modified $CsPbI_3$ (Pb:Zr=1:1) top-emitting Pe-QLEDs at different viewing angles. (b) CIE coordinate of the EL emission.

Table S3. EL characteristics, including the efficiency roll-off, of several recently reported green and red emitting Pe-LEDs.

Emitting material	**EL peak (nm)**	**EQE_{max} (%)**	**EQE (%) @100 mA cm^{-2}**	**EQE (%) @500 mA cm^{-2}**	**Efficiency roll-off (%)**	**Reference**
$CsPbI_3$ QDs	*686*	*13.7*		*12.5*	*8.7*	*This work*
$BA_2(CsPbBr_3)_{n-1}PbBr_4$-PEO films	514	8.42	6.5		22.8	[7]
$MAPbBr_3$ QDs	524	12.9	6.0		53.5	[8]
$CsPbBr_3$ QDs	512	15.17	6.0		47.3	[9]
$CsPbBr_3$ films	518	10.5	4.5		52.4	[10]
$CsPbBr_3$ films		20.3	9.0		46.8	[11]
$CsPbBr_3$/MABr films	525	20.3	12.0		40.9	[12]
$MAPbBr_3$ films	540	21.8	13.7		37.2	[13]
$Cs_{0.2}FA_{0.8}PbI_{2.8}Br_{0.2}$ films	752	17.6		9.0	48.8	[14]
$CsPbI_3$ QDs	691	13.5		4.2	68.9	[15]
$NFPI_7$ films	790	12.7		10	21.3	[16]
$CsPbI_3$ QDs	691	11.8		8	32.3	[17]
$CsPbI_3$ QDs	678	5.92		3.3	44.2	[18]
$CsPbI_3$ QDs	682	15.1		5.5	63.6	[19]
$FAPbI_3$ films	800	21.6		15.5	28.2	[20]

Table S4. EL performance of recently reported red emitting Pe-QLEDs.

Material	EL peak (nm)	EQE_{max} (%)	L_{max} (cd m^{-2})	Reference
$CsPbI_3$	*686*	*13.7*	*14725*	*This work*
$MAPbX_3$	640	0.53	986	[21]
$CsPbI_3$	698	5.7	206	[22]
$CsPb(Br/I)_3$	648	6.3	2216	[23]
$CsPbI_3$	688	5.02	748	[24]
$CsPbI_3$	683	7.3	100	[25]
$CsPb(Br/I)_3$	650	0.05	30	[26]
$CsPbI_3$	690	14.08	1444	[27]
$CsPb(Br/I)_3$	645	21.3	794	[28]
$CsPb_{0.64}Zn_{0.36}I_3$	682	15.1	2202	[19]
$CsPbI_3$	678	5.92	1250	[18]

References

(1) Wen, Q.; Kershaw, S. V.; Kalytchuk, S.; Zhovtiuk, O.; Reckmeier, C.; Vasilevskiy, M. I.; Rogach, A. L. Impact of D_2O/H_2O Solvent Exchange on the Emission of HgTe and CdTe Quantum Dots: Polaron and Energy Transfer Effects. *ACS Nano* **2016,** *10*, 4301-4311.

(2) Wang, S.; Wang, Y.; Zhang, Y.; Zhang, X.; Shen, X.; Zhuang, X.; Lu, P.; Yu, W. W.; Kershaw, S. V.; Rogach, A. L. Cesium Lead Chloride/Bromide Perovskite Quantum Dots with Strong Blue Emission Realized via a Nitrate-Induced Selective Surface Defect Elimination Process. *J. Phys. Chem. Lett.* **2019,** *10*, 90-96.

(3) Tian, Y.; Merdasa, A.; Peter, M.; Abdellah, M.; Zheng, K.; Ponseca, C. S.; Pullerits, T.; Yartsev, A.; Sundström, V.; Scheblykin, I. G. Giant Photoluminescence Blinking of Perovskite Nanocrystals Reveals Single-Trap Control of Luminescence. *Nano Lett.* **2015,** *15*, 1603-1608.

(4) Swarnkar, A.; Chulliyil, R.; Ravi, V. K.; Irfanullah, M.; Chowdhury, A.; Nag, A. Colloidal $CsPbBr_3$ Perovskite Nanocrystals: Luminescence beyond Traditional Quantum Dots. *Angew. Chem. Int. Ed.* **2015,** *54*, 15424-15428.

(5) Ebenstein, Y.; Mokari, T.; Banin, U. Fluorescence quantum yield of CdSe/ZnS nanocrystals investigated by correlated atomic-force and single-particle fluorescence microscopy. *Appl. Phys. Lett.* **2002,** *80*, 4033-4035.

(6) Yao, J.; Larson, D. R.; Vishwasrao, H. D.; Zipfel, W. R.; Webb, W. W. Blinking and nonradiant dark fraction of water-soluble quantum dots in aqueous solution. *Proc. Natl. Acad. Sci. U. S. A.* **2005,** *102*, 14284-14289.

(7) Wang, Z.; Wang, F.; Sun, W.; Ni, R.; Hu, S.; Liu, J.; Zhang, B.; Alsaed, A.; Hayat, T.; Tan, Z. a. Manipulating the Trade-off Between Quantum Yield and Electrical Conductivity for High-Brightness Quasi-2D Perovskite Light-Emitting Diodes. *Adv. Funct. Mater.* **2018,** *28*, 1804187.

(8) Yan, F.; Xing, J.; Xing, G.; Quan, L.; Tan, S. T.; Zhao, J.; Su, R.; Zhang, L.; Chen, S.; Zhao, Y. Highly Efficient Visible Colloidal Lead-Halide Perovskite Nanocrystal Light-Emitting Diodes. *Nano Lett.* **2018,** *18*, 3157-3164.

(9) Yuan, S.; Wang, Z.-K.; Zhuo, M.-P.; Tian, Q.-S.; Jin, Y.; Liao, L.-S. Self-Assembled High Quality CsPbBr3 Quantum Dot Films toward Highly Efficient Light-Emitting Diodes. *ACS Nano* **2018,** *12*, 9541-9548.

(10) Wang, H.; Zhang, X.; Wu, Q.; Cao, F.; Yang, D.; Shang, Y.; Ning, Z.; Zhang, W.; Zheng,

W.; Yan, Y.; Kershaw, S. V.; Zhang, L.; Rogach, A. L.; Yang, X. Trifluoroacetate induced small-grained $CsPbBr_3$ perovskite films result in efficient and stable light-emitting devices. *Nat. Commun.* **2019,** *10*, 665.

(11) Shen, Y.; Cheng, L.-P.; Li, Y.-Q.; Li, W.; Chen, J.-D.; Lee, S.-T.; Tang, J.-X. High-Efficiency Perovskite Light-Emitting Diodes with Synergetic Outcoupling Enhancement. *Adv. Mater.* **2019,** *31*, 1901517.

(12) Lin, K.; Xing, J.; Quan, L. N.; de Arquer, F. P. G.; Gong, X.; Lu, J.; Xie, L.; Zhao, W.; Zhang, D.; Yan, C.; Li, W.; Liu, X.; Lu, Y.; Kirman, J.; Sargent, E. H.; Xiong, Q.; Wei, Z. Perovskite light-emitting diodes with external quantum efficiency exceeding 20 percent. *Nature* **2018,** *562*, 245-248.

(13) Park, M.-H.; Park, J.; Lee, J.; So, H. S.; Kim, H.; Jeong, S.-H.; Han, T.-H.; Wolf, C.; Lee, H.; Yoo, S.; Lee, T.-W. Efficient Perovskite Light-Emitting Diodes Using Polycrystalline Core–Shell-Mimicked Nanograins. *Adv. Funct. Mater.* **2019,** *29*, 1902017.

(14) Zhao, L.; Rolston, N.; Lee, K. M.; Zhao, X.; Reyes-Martinez, M. A.; Tran, N. L.; Yeh, Y.-W.; Yao, N.; Scholes, G. D.; Loo, Y.-L.; Selloni, A.; Dauskardt, R. H.; Rand, B. P. Influence of Bulky Organo-Ammonium Halide Additive Choice on the Flexibility and Efficiency of Perovskite Light-Emitting Devices. *Adv. Funct. Mater.* **2018,** *28*, 1802060.

(15) Lu, M.; Zhang, X.; Zhang, Y.; Guo, J.; Shen, X.; Yu, W. W.; Rogach, A. L. Simultaneous Strontium Doping and Chlorine Surface Passivation Improve Luminescence Intensity and Stability of $CsPbI_3$ Nanocrystals Enabling Efficient Light-Emitting Devices. *Adv. Mater.* **2018,** *30*, 1804691.

(16) Zou, W.; Li, R.; Zhang, S.; Liu, Y.; Wang, N.; Cao, Y.; Miao, Y.; Xu, M.; Guo, Q.; Di, D.; Zhang, L.; Yi, C.; Gao, F.; Friend, R. H.; Wang, J.; Huang, W. Minimising efficiency roll-off in high-brightness perovskite light-emitting diodes. *Nat. Commun.* **2018,** *9*, 608.

(17) Zhang, X.; Lu, M.; Zhang, Y.; Wu, H.; Shen, X.; Zhang, W.; Zheng, W.; Colvin, V. L.; Yu, W. W. PbS Capped $CsPbI_3$ Nanocrystals for Efficient and Stable Light-Emitting Devices Using p–i–n Structures. *ACS Cent. Sci.* **2018,** *4*, 1352-1359.

(18) Yao, J.-S.; Ge, J.; Wang, K.-H.; Zhang, G.; Zhu, B.-S.; Chen, C.; Zhang, Q.; Luo, Y.; Yu, S.-H.; Yao, H.-B. Few-Nanometer-Sized α-$CsPbI_3$ Quantum Dots Enabled by Strontium Substitution and Iodide Passivation for Efficient Red-Light Emitting Diodes. *J. Am. Chem. Soc.*

2019, *141*, 2069-2079.

(19) Shen, X.; Zhang, Y.; Kershaw, S. V.; Li, T.; Wang, C.; Zhang, X.; Wang, W.; Li, D.; Wang, Y.; Lu, M.; Zhang, L.; Sun, C.; Zhao, D.; Qin, G.; Bai, X.; Yu, W. W.; Rogach, A. L. Zn-Alloyed $CsPbI_3$ Nanocrystals for Highly Efficient Perovskite Light-Emitting Devices. *Nano Lett.* **2019,** *19*, 1552-1559.

(20) Xu, W.; Hu, Q.; Bai, S.; Bao, C.; Miao, Y.; Yuan, Z.; Borzda, T.; Barker, A. J.; Tyukalova, E.; Hu, Z.; Kawecki, M.; Wang, H.; Yan, Z.; Liu, X.; Shi, X.; Uvdal, K.; Fahlman, M.; Zhang, W.; Duchamp, M.; Liu, J.-M.; Petrozza, A.; Wang, J.; Liu, L.-M.; Huang, W.; Gao, F. Rational molecular passivation for high-performance perovskite light-emitting diodes. *Nat. Photonics* **2019,** *13*, 418-424.

(21) Deng, W.; Xu, X.; Zhang, X.; Zhang, Y.; Jin, X.; Wang, L.; Lee, S. T.; Jie, J. Organometal Halide Perovskite Quantum Dot Light-Emitting Diodes. *Adv. Funct. Mater.* **2016,** *26*, 4797-4802.

(22) Li, G.; Rivarola, F. W.; Davis, N. J.; Bai, S.; Jellicoe, T. C.; De, l. P. a. F.; Hou, S.; Ducati, C.; Gao, F.; Friend, R. H. Highly Efficient Perovskite Nanocrystal Light-Emitting Diodes Enabled by a Universal Crosslinking Method. *Adv. Mater.* **2016,** *28*, 3528-3534.

(23) Zhang, X.; Sun, C.; Zhang, Y.; Wu, H.; Ji, C.; Chuai, Y.; Wang, P.; Wen, S.; Zhang, C.; Yu, W. W. Bright Perovskite Nanocrystal Films for Efficient Light-Emitting Devices. *J. Phys. Chem. Lett.* **2016,** *7*, 4602-4610.

(24) Pan, J.; Shang, Y.; Yin, J.; De Bastiani, M.; Peng, W.; Dursun, I.; Sinatra, L.; El-Zohry, A. M.; Hedhili, M. N.; Emwas, A.-H.; Mohammed, O. F.; Ning, Z.; Bakr, O. M. Bidentate Ligand-Passivated $CsPbI_3$ Perovskite Nanocrystals for Stable Near-Unity Photoluminescence Quantum Yield and Efficient Red Light-Emitting Diodes. *J. Am. Chem. Soc.* **2018,** *140*, 562-565.

(25) Si, J.; Liu, Y.; He, Z.; Du, H.; Du, K.; Chen, D.; Li, J.; Xu, M.; Tian, H.; He, H. Efficient and High-Color-Purity Light-Emitting Diodes Based on In-Situ Grown Films of $CsPbX_3$ (X = Br, I) Nanoplates with Controlled Thicknesses. *ACS Nano* **2017,** *11*, 11100-11107.

(26) Yassitepe, E.; Yang, Z.; Voznyy, O.; Kim, Y.; Walters, G.; Castañeda, J. A.; Kanjanaboos, P.; Yuan, M.; Gong, X.; Fan, F. Amine-Free Synthesis of Cesium Lead Halide Perovskite Quantum Dots for Efficient Light-Emitting Diodes. *Adv. Funct. Mater.* **2016,** *26*, 8757-8763.

(27) Li, G.; Huang, J.; Zhu, H.; Li, Y.; Tang, J.-X.; Jiang, Y. Surface Ligand Engineering for Near-Unity Quantum Yield Inorganic Halide Perovskite QDs and High-Performance QLEDs. *Chem. Mater.* **2018,** *30*, 6099-6107.

(28) Chiba, T.; Hayashi, Y.; Ebe, H.; Hoshi, K.; Sato, J.; Sato, S.; Pu, Y.-J.; Ohisa, S.; Kido, J. Anion-exchange red perovskite quantum dots with ammonium iodine salts for highly efficient light-emitting devices. *Nat. Photonics* **2018,** *12*, 681-687.